ADVANCED MATERIALS TECHNOLOGIES
www.advmattechnol.de

Magnetically Actuable Complex-Shaped Microgels for Spatio-Temporal Flow Control

Lea Steinbeck, Dominik L. Braunmiller, Hanna J. M. Wolff, Vincent Huettche, Julia Wang, Matthias Wessling, Jérôme J. Crassous, and John Linkhorst**

Complex-shaped microgels are promising building blocks for soft metamaterials. Their active and remote orientational control provides significant potential in architecting them in time and space. This work describes the use of magnetically actuable microgels of complex shape for spatio-temporal flow control and showcases the concept for microfluidic impellers. First, the fabrication of complex-shaped magnetically actuable poly(ethylene glycol) diacrylate based microgels via stop-flow lithography is presented. The microgels comprise a pre-programmed magnetic moment set by pre-aligned maghemite nanospindles during the fabrication step. This feature allows the microgels to be positioned in a static magnetic field and rotate under application of a rotating external field. The dependence of the magnetic field rotation rate and strength, maghemite content, and microgel shape on the magnetic response of the microgels is comprehensively quantified. Finally, the magnetic complex-shaped microgels are integrated as actuable impellers in a microfluidic chip. The microgels are positioned in space by polymerizing them around fixed poly(dimethylsiloxane) (PDMS) pillars. Free rotation around the PDMS pillar is achieved due to the oxygen inhibition layer at the chip and pillar surface. The versatility of the fabrication methodology is showcased by the investigation of in-chip mixing in a microfluidic device consisting of soft responsive impellers.

1. Introduction

Metamaterials, a class of materials with anisotropic properties, have gained increased attention over the past years. These materials can go beyond a static function and provide a dynamic response over time by following a pre-programmed trajectory.[1] To achieve an architected structure, building blocks with diverse properties are integrated into a single building block or assembled in a superstructure, responding to diverse stimuli, comprising mechanical,[2] optical,[3] electrical,[4] and magnetic responsiveness.[5–8] Aside from static, these materials allow for spatio-temporal flow control. A whole new field of autonomous flow control was introduced through the pioneering work of Beebe et al.[9] Previously published flow control devices range from pH-responsive hydrogel valves[9,10] over guidable colloids[11,12] to pumping approaches.[13–15] Thus, being able to custom design the building blocks is essential. In this respect, microgels are highly promising materials as they allow free-form fabrication and are highly tailorable in terms of mechanical and chemical properties and gradients thereof.[16–19] Implementing magnetic responsiveness into microgels is of substantial interest, as the magnetic field can easily penetrate, for example, tissue without adverse effects. As an example, the magnetic response of rod-shaped microgels can be used to remotely control their orientation during the scaffold build-up to guide cell growth.[20] Besides allowing to control the structural assembly,[21–23] magnetic responsive building blocks are ultimately expected to provide the possibility to study mechanotransduction similar to light-responsive soft hydrogels.[24]

Several examples of the incorporation of magnetic materials into hydrogels and microgels by various fabrication methods are reported in the literature. Anisometric magnetic microgels have been synthesized among other techniques by particle replication in non-wetting template (PRINT),[20,21,25,26] maskless lithography,[27] and stop-flow lithography (SFL).[28–30] The incorporated magnetic materials are mostly based on iron oxide,[31,32] more precisely magnetite,[25,30] for example, in the form of superparamagnetic iron oxide nanoparticles (SPIONs),[21] colloidal

L. Steinbeck, H. J. M. Wolff, V. Huettche, M. Wessling, J. Linkhorst
Chemical Process Engineering AVT.CVT
RWTH Aachen University
Forckenbeckstr. 51, 52074 Aachen, Germany
E-mail: manuscripts.cvt@avt.rwth-aachen.de

D. L. Braunmiller, J. Wang, J. J. Crassous
Institute of Physical Chemistry IPC
RWTH Aachen University
Landoltweg 2, 52074 Aachen, Germany
E-mail: crassous@pc.rwth-aachen.de

M. Wessling
DWI - Leibniz Institute for Interactive Materials
Forckenbeckstr. 50, 52074 Aachen, Germany

The ORCID identification number(s) for the author(s) of this article can be found under https://doi.org/10.1002/admt.202300044

DOI: 10.1002/admt.202300044

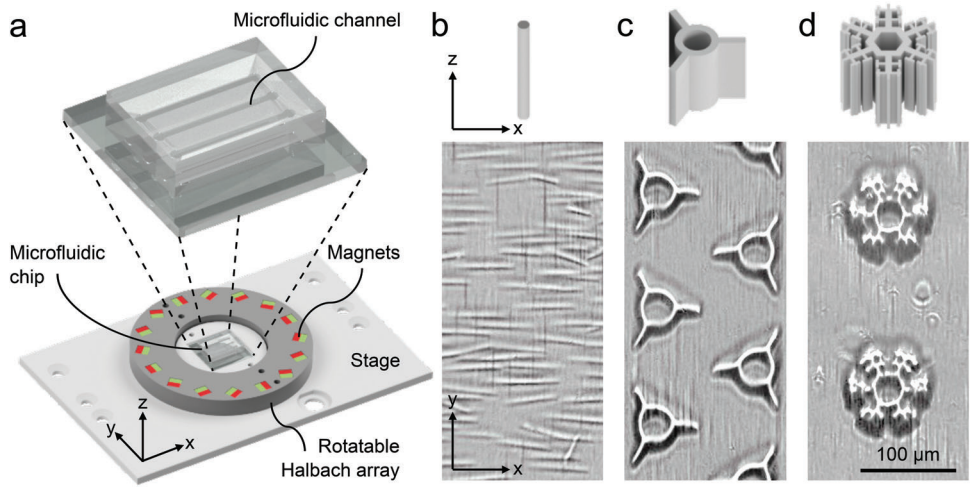

Figure 1. Fabrication of PEGDA microgels with integrated maghemite spindles. a) Setup of the microgel fabrication (b–d) with the applied shapes and aligned maghemite nanospindles during microgel fabrication: b) rod, c) impeller, and d) snowflake microgels.

nanocrystal clusters,[27] or ferrofluids.[29] The magnetic nanoparticles are usually dispersed in the reaction mixture and integrated during the polymerization of the hydrogels.[20,21,25] Magnetic microgel rods loaded with SPIONs fabricated via PRINT were found to align exclusively along the magnetic field as a consequence of their shape anisotropy.[22] To pre-program the magnetic response and pre-define the magnetic moment of the microgels, only a few studies have explored the possibility of fabricating anisometric microgels under the presence of an external magnetic field.[23,26,27,33]

Recently, some of the authors have introduced the use of magnetically pre-aligned maghemite nanospindles as an alternative for SPIONs to direct the orientation of microgels.[23,33] Indeed, maghemite nanospindles exhibit a fixed magnetic moment expected along their major axis, in contrast to the freely rotating magnetic moment of the superparamagnetic SPIONs.[34] The γ-Fe_2O_3 maghemite nanospindles were obtained through the reduction of α-Fe_2O_3 hematite particles into Fe_3O_4 magnetite and re-oxidation at high temperatures. By applying an external magnetic field, maghemite nanospindles first align at a low field and form dipolar chains with increasing field strength.[23,34] Due to their high magnetic response, permanent magnetic moment, and anisotropic shape, maghemite nanospindles were therefore incorporated into PRINT rod-shaped microgels. This incorporation allowed to pre-program their magnetic properties in 3D under static or rotating magnetic fields, where the magnetic properties were found to depend directly on the nanospindle orientation within the microgels.[23,33] However, the PRINT fabrication process only allows to produce a limited amount of microgels.

In the present work, the high throughput fabrication of magnetic microgels via SFL is demonstrated, extending the maghemite-loaded rod-shaped microgels presented in the former study[23] to complex-shaped microgels. For this purpose, pre-aligned maghemite nanospindles are incorporated into poly(ethylene glycol) diacrylate (PEGDA) microgels during the polymerization in a homogeneous magnetic field created by a Halbach array. Several microgels are synthesized with different shapes and polymerization parameters. Their magnetic response is investigated under rotating magnetic fields to determine the influence of the microgel shape, the maghemite content, and the applied magnetic field, taking advantage of their optical properties. Finally, the applications of the anisometric magnetic microgels as freely rotating actuators and fixed impellers inside a microfluidic device are evaluated to showcase their applications for actuable microfluidics.

2. Results and Discussion

2.1. Magnetic Microgel Fabrication

To achieve anisometric, magnetically actuable building blocks, maghemite nanospindles were integrated into anisometric PEGDA microgels using stop-flow lithography (SFL). The nanospindles added to the precursor solution were first aligned by the magnetic field of a Halbach array in a microfluidic channel as schematically illustrated in **Figure 1**a. The microfluidic chip was positioned in all three dimensions in the center of the Halbach array to ensure a homogeneous magnetic field in the polymerization area. In addition, the chip platform allows a controlled orientation of the surrounding Halbach array, enabling to set the maghemite orientation within the microfluidic channel. This way, complex-shaped microgels with a pre-defined magnetic moment were synthesized by SFL.

To analyze the magnetic response, rod-, impeller-, and snowflake-shaped microgels were produced. In Figure 1b–d, the different microgels are displayed both as a schematic drawing and by a bright field micrograph during fabrication (xy plane). In contrast to the images of the impellers and snowflakes, the rods were manually tilted to the side (from xz to xy plane) to visualize their rod shape in the micrograph. The applied magnetic field during fabrication causes an alignment of the maghemite spindles in the y-direction perpendicular to the microgels' longitudinal z-axis. Thus, when lying, the rods align perpendicular to the still applied magnetic field due to their pre-defined magnetic moment (Figure 1b). This pre-defined magnetic moment is independent of the anisometry of the microgels, but only de-

pends on the maghemite nanospindle orientation within the microgels. The nanospindles have in contrast to spherical nanoparticles a direction-dependent magnetic response. Thus, by integrating maghemite nanospindles into the microgels, the direction of the magnetic moment of the microgels can be pre-defined by the applied magnetic field during fabrication. The rod-shaped microgels were fabricated with and without an applied magnetic field to investigate the influence of the maghemite alignment within the microgels. The snowflake-shaped microgels were fabricated with differing polymerization parameters to analyze the influence of fabrication conditions on the magnetic properties. For the impeller-shaped microgels, the maghemite content was varied to test its effect on the microgels' magnetic moment. The impellers were additionally characterized by scanning electron microscopy (SEM) to evidence the presence of the dipolar chains as discussed in supporting information (see Figure S2, Supporting Information).

In total, 11 microgel samples were fabricated whose magnetic response was analyzed in terms of microgel shape, maghemite spindle alignment, polymerization parameters, maghemite content, and magnetic field strength. Whereas the influence of the microgel shape, the maghemite content, and the field strength are discussed in detail below, the results for investigation of the maghemite alignment and polymerization parameter can be stated briefly: The alignment of the maghemite spindles in the reaction solution showed to be crucial to enable a rotation of the microgels. Microgels fabricated without alignment of maghemite spindles, meaning fabrication without a magnetic field, do not align uniformly to the magnetic field and show a weak magnetic response. In contrast, pre-aligning the nanospindles leads to a significant improvement of the magnetic response and enables to orient the microgels. In terms of the polymerization parameters, two polymerization parameter extremes were used during fabrication. For one sample long exposure time and low radiant flux were applied, for the other short exposure time and high radiant flux. The variation of the polymerization parameters does not influence the magnetic response of the fabricated microgels. Regarding the three remaining factors, microgel shape, maghemite content, and field strength, the magnetic response was investigated in detail by determining the rotation rate of the different magnetic microgels as a function of the rotation rate of the magnetic field.

2.2. Magnetic Responsiveness

Considering a ferromagnetic system in a Newtonian fluid under a magnetic field rotating with the angular frequency ω, the equation of motion reads:

$$\gamma\left(\omega + \frac{d\theta}{dt}\right) = \mu B \cdot sin\theta \tag{1}$$

where γ is the drag coefficient and θ the angle between the magnetic moment of the system μ and the applied field B. This expression describes the balance of the torques set by the rotation of the system in the fluid and the magnetic torque. The system rotates synchronously as long as $d\theta\ dt^{-1} \approx 0$, which allows to define the critical angular frequency $\omega_C = \mu B\ \gamma^{-1}$. For $\omega > \omega_C$, the system cannot continuously follow the field and start to tumble. Hence, the magnetic moment is not able to follow the field and θ becomes time-dependent. Measuring the field and angular frequency dependence of ω allows to characterize the magnetic response of the particles.

An interesting feature of the incorporated nanoparticle chains can be used to determine the angular frequency of the microgels. As the dipolar chains formed by the maghemite spindles (Figures S1 and S2, Supporting Information) polarize the light, the orientation of the chains can be determined using cross-polarization microscopy (**Figure 2**a–d). Thereby, a linear polarizer and an analyzer, orientated perpendicular to each other, are positioned before and after the sample on a microscope. Light cannot pass through both without being polarized by the sample. The intensity I_N of the transmitted light depends on the angle α between the orientation of the polarizer and the dipolar chains (Figure 2b). This feature is used to determine the angular frequency by the maxima of the intensity profile—A full rotation of the microgels with the entrapped maghemite chains is indicated by two larger and two smaller maxima (Figure 2e). While working perfectly in the synchronous regime (Figure 2f), in the asymmetric rotation regime, the intensity profile is influenced by the tumbling of the microgels (Figure 2g). Depending on the degree of rattling, additional manual evaluation was performed.

The rotation behavior of a single impeller-shaped microgel is exemplarily shown in **Figure 3**a. With an increasing rotation rate of the magnetic field ω_{MF}, the rotation of the microgel ω increases linearly up to the critical rotation rate ω_C. This linear increase represents the synchronous rotation regime, in which the microgel rotates in sync with the magnetic field (Video S1, Supporting Information). The angle ω between magnetic torque of the microgel and the orientation of the magnetic field is constant. The rotation behavior changes above the critical rotation rate. At this point, the microgels start to tumble and, as a result, ω drops significantly below ω_{MF} (Video S2, Supporting Information). The friction and drag forces are greater than the magnetic torque in the asynchronous rotation regime ($\omega_{MF} > \omega_C$). This increases the angle θ between the magnetic field and the magnetic moment. Before the magnetic field overtakes the magnetic moment, there is a change in direction of the microgel rotation. When the magnetic field overtakes the magnetic moment of the microgel, another change in the direction of rotation leads to further rotation in the original direction. These back-and-forth oscillations are here characterizing the tumbling regime. The tumbling affects the rotational behavior, but the overall rotation proceeds in the direction of the magnetic field at a lower rate, which can be determined as described above.

2.3. Influence of Microgel Shape, Maghemite Content, and Magnetic Field Strength on the Magnetic Responsiveness

In addition to ω_{MF}, the magnetic response of the microgels depends on a variety of parameters, for example, magnetic field strength, maghemite content, and shape of the microgels. In order to determine the average magnetic response, around 20 microgels are considered and their mean rotation rates ω are summarized in Figure 3b–d. Generally, the response of the different microgels shows larger variations from microgel to microgel for

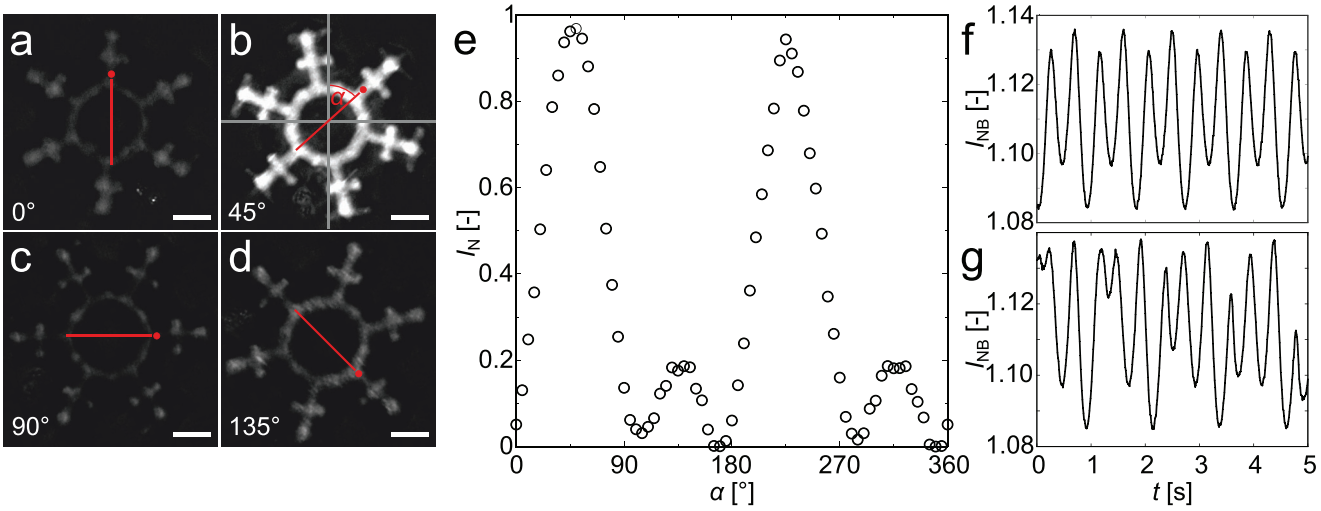

Figure 2. Optical analysis of light polarization via magnetic rotation of maghemite nanospindles incorporated in snowflake-shaped microgels. a–d) Cross-polarization micrographs of a microgel with incorporated maghemite chains orientated at different angles α to the polarizer. The transmitted intensity I changes depending on α. The grey lines indicate the orientation of the polarizer; the red lines with the dot corresponds to the orientations of the maghemite chains within the microgel. Scale bars: 20 µm. e) Intensity I_N profile of the rotating microgel normalized on the maximum and minimum intensity. A full rotation is indicated by two large and two small maxima at 45° (and 225°) and 135° (and 315°), respectively. f) Intensity profile of a synchronously rotating microgel with a motor speed f_{MF} and microgel rotation rate of 66.7 rpm. g) Intensity profile of an asynchronously rotating microgel with a motor speed f_{MF} of 73.3 rpm and a microgel rotation rate of 48.2 rpm. The additional intensity fluctuation is caused by a tumbling motion of the microgel. The intensity I_{NB} in (f) and (g) is normalized by the background of the image.

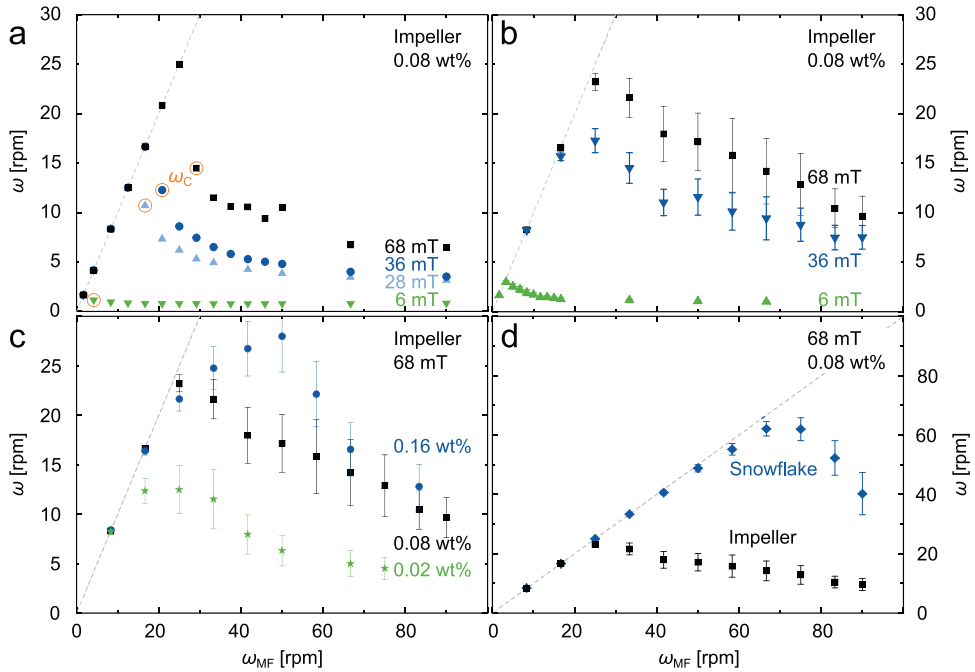

Figure 3. Magnetic response of the magnetic microgels measured as their microgel rotation rate ω as function of the field rotation rate ω_{MF}. a) Magnetic response of a single impeller-shaped microgel in dependence on the rotation rate ω_{MF} and strength of the magnetic field. The critical rotation rate ω_C indicates the transition between the synchronous and the asynchronous rotation regime ( ). b–d) Mean magnetic response of complex-shaped microgels ($n \approx 20$) to rotating magnetic fields of varying forces with regard to b) field strength, c) maghemite content, and d) shape.

higher microgel rotation rates and field strengths as for the critical rotation rate. Possible reasons for this variation are different contact areas or gap sizes between microgel and glass surface, as different friction or shear forces influence the rotation rates. Furthermore, there might be inhomogeneities in the nanospindle loadings inside the microgels due to unavoidable inhomogeneous chain formation during the production. Accordingly, the critical rotation rate ω_C was not determined from the mean ω-values but rather from the individual data sets, as shown in Figure 3a.

With an increasing magnetic field strength B, the mean rotation rate ω of impeller-shaped microgels with a maghemite loading of 0.08 wt% increases as shown in Figure 3b. While the data for 6 mT exhibit the above-described linear increase of the rotation rate in the synchronous regime and a non-linear decrease in the asynchronous regime, the mean curves for higher field strengths show a more linear decrease. This linear decay is a result of the strong variation of ω_C for higher field strengths (Figure S3a, Supporting Information). The mean value of ω_C increases from 5.3 ± 0.3 rpm at 6 mT to 22.2 ± 1.3 rpm (36 mT) and 32.2 ± 1.8 rpm (68 mT), respectively. The rotation rate seems to reach a saturation value at some point above 68 mT, as the difference between 6 and 36 mT with 16.9 rpm is significantly larger than between 36 and 68 mT (10 rpm). As the magnetic torque is directly depending on the mass of the magnetic material in the microgels, a higher maghemite loading and a larger microgel shape are expected to increase the magnetic response of the composite microgels. The mean value of ω_C at 68 mT of impeller-shaped microgels increases from 21.5 ± 2.3 rpm with a nanoparticle content of 0.02 wt% to 32.2 ± 1.8 rpm (0.08 wt%) and 34.2 ± 2.8 rpm (0.16 wt%), respectively. While a higher maghemite content in the precursor solution increases the microgels' magnetic response, it also increases the inhomogeneity of the response to the magnetic field as shown in Figure 3c. The transition between synchronous regime and asynchronous regime varies stronger for 0.16 wt% than for the lower contents (Figure S3b, Supporting Information). The higher contents might lead to a less defined chain-structure inside the microgels, resulting in more inhomogeneous magnetic properties and a lower effect of the magnetic filler content in respect to the field.

The shape of the produced microgels influences on the one hand the magnetic moment by the volume of the microgel. On the other hand, the viscous torque as well as friction and shear forces at the surface of the microgels counteract to the magnetic torque. For this investigation, impeller- and snowflake-shaped microgels with the same maghemite loading of 0.08 w% are actuated with a magnetic field of 68 mT (Figure 3d). The magnetic response of the snowflake-shaped microgels with a mean critical rotation rate at 79.8 ± 3.2 rpm is significantly higher than for impeller-shaped microgels (ω_C = 32.2 ± 1.8 rpm). As the magnetic torque is proportional to the used magnetic material (Equation (1)) and thus proportional to the volume of the nanoparticles, the magnetic response is expected to increase proportionally with the volume of the microgel. As the snowflake-shaped microgels have a estimated volume of 178 ± 14 × 10^3 µm^3 and the impeller-shaped of 97 ± 2 × 10^3 µm^3, this relates to a ratio of around 2:1 and an expected stronger magnetic response of the snowflakes. The magnetic torque is counteracted by the viscous torque and the frictional and shear forces on the surface of the microgels. The snowflake-shaped microgels have a surface area on the bottom side of 2138 ± 164 µm^2 and the impeller-shaped microgels of 1048 ± 21 µm^2. Again, this relates to a ratio of 2:1. Since the critical rotation rate is over two times higher for the snowflake-shaped microgels, the contribution of the magnetic torque is stronger than the friction forces. As neither of these forces nor the exact surface of complex shapes like snowflakes can be easily quantified, the influence of the shape cannot be clarified conclusively at this point. The fabricated rod-shaped microgels also respond to a magnetic field, but show a significantly weaker magnetic responsiveness. The magnetic response of rod-shaped microgels produced with another fabrication method was analyzed in detail in a previous work[23] and, therefore, not included here in more detail. To show the use of these microgels as impellers, some of these experiments were repeated with hollow polystyrene (PS) tracer particles inside the sample cell. Hereby, the flow generated by impellers rotating synchronously with the field was analyzed by tracking the position of the PS particles as discussed in the supporting information (Section S3 and Figures S4–S7, Supporting Information) Thereby, it could be shown that the rotating microgels create a strong flow influencing a large area, depending on their rotation rates. Such flow and its potential application for micro-rheometry will be investigate in more detail in a future study.

2.4. In-Chip Integration of Actuable Complex-Shaped Microgels

The fixed axis rotation of magnetic microgels was directly implemented by integrating them via SFL into a microfluidic chip with PDMS pillars. Thus, the internal flow can be selectively influenced by the rotating microgels working as impellers.

To fixate the rotating impellers inside the channel, a microfluidic chip with pillars was fabricated. The pillars serve as fixation points for the impellers, allowing the microgels to rotate around a fixed axis. **Figure 4**a shows a SEM micrograph of the microfluidic channel made of PDMS in which the pillars are arranged in a square lattice.

In order to find the right combination of diameters for the integrated pillars and surrounding impellers, two counteracting aspects have to be considered. On the one hand, the distance between pillar and surrounding microgel should be as small as possible to ensure a smooth and homogeneous rotation. On the other hand, the pillars with microgels around them have to be resistant against the pressure during fluid flushing and the impeller wall needs to hold the pressure as well. As a result of the oxygen inhibition layer around the pillars during polymerization of impellers, the pillar diameter has to be significantly smaller than the inner diameter of the impeller shape. Otherwise, the impellers' wall thickness is reduced by the oxygen inhibition in comparison to the designated shape. Unfortunately, a larger inner diameter of the impellers allows tumbling and movement of the impellers around the pillars other than rotation. To achieve a uniform short distance between pillar and microgel, microgel shapes without a pre-defined inner diameter are used for the fabrication around the pillars. Both impeller shapes, with and without inner diameter, are displayed in Figure S8(I), Supporting Information. Due to the oxygen inhibition layer surrounding the PDMS pillars, the microgels do not stick to the pillars. This results in the

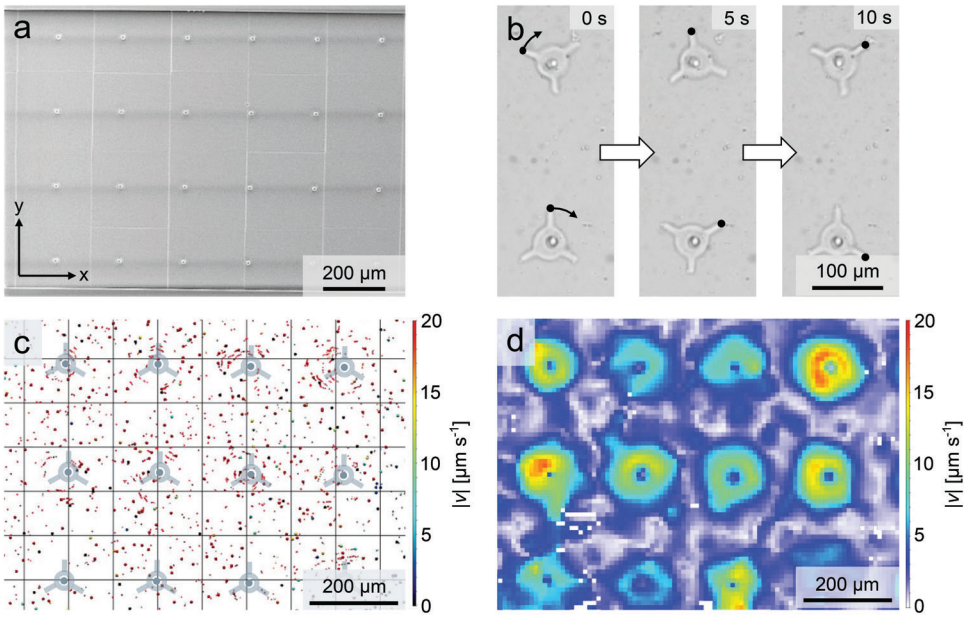

Figure 4. Actuable microfluidics and rotation analysis. a) SEM micrograph of the microfluidic channel with PDMS pillars. b) Time series of clockwise rotating impellers around pillars in-chip. c) Micro particle tracking velocimetry (µPTV) flow analytic showing particle transport induced by rotating impellers which are schematically illustrated. d) µPTV image with analyzed flow direction and velocities.

same microgel shape as for microgels with pre-defined inner diameter, but the distance to the pillars is reduced and even. Thus, the pillar diameter is kept small to ensure stable impeller walls, and the distance to the microgels is set by the oxygen inhibition layer. By using a microgel shape without inner diameter, the microgels are stable against fluid flushing and enable fixed rotation around the pillars.

For microgel fabrication, the channel is flushed with monomer solution containing PEGDA, lithium phenyl-2,4,6-trimethylbenzoylphosphinate (LAP), maghemite nanospindles, 4-methoxyphenole (MEHQ), and water. The positioning of the microgel polymerization areas in the exact spots of the pillars inside the channel is crucial to successfully fabricate homogeneous, intact, and rotatable microgels. Two aspects were identified as obstacles to rotation: adhesion of the microgels to the channel and microgel swelling. To address these challenges, different flushing solutions were tested. To avoid further polymerization after fabrication, the reaction solution is exchanged with an aqueous solution containing 1 wt% MEHQ to hinder a potential ongoing polymerization by binding free radicals. Pure water as flushing solution resulted in restricted or even no movement of the impellers and was, therefore, not used. To prevent adhesion, the surfactant polyoxyethylene (20) sorbitan monolaurate (Tween-20) is widely used in microfluidics in droplet makers, but also to reduce surface interaction in pipette tips. [28] The addition of 0.05 v% Tween -20 to the flushing solution was found to reduce sticking to the channel walls and allowed for a better rotation stability. To avoid swelling and counteract an increase of the microgel size, the osmotic pressure in the flushing solution was increased. Polymers or salts have previously been shown to effectively reduce swelling. [35–37] In contrast to salts, the usage of PEGDA avoids introducing an additional component to the experimental system. Thus, PEGDA was added to the flushing solution with a concentration of 40 wt%, twice as high as in the reaction solution, allowing to keep the size of the impellers constant. However, the concentration of PEGDA cannot be increased too much, as the microgels would be constricted at the axis of rotation if they shrink further. The final flushing solution used in rotation experiments consists of Tween -20, PEGDA (average molecular weight of 575 Da), MEHQ, and water, preventing further polymerization, swelling, and sticking of the microgels. Additionally, an increased pressure during rotation experiments significantly increases the rotation ability, having an impact on sticking and swelling. The pressure widens the whole channel, resulting in more space for swollen microgels and possibly weaken the obstructive PDMS microgel connection.

To induce a rotation of the fabricated microgel impellers, the magnetic field has to be aligned with the chip. The strongest area of the Halbach array, which is in its center, needs to be in the same height as the microgels within the microfluidic channel, as discussed in Section 2.1. Ideally, the microgels are in the center of the Halbach array regarding all three dimensions. This ensures that the strongest and most homogeneous part of the magnetic field influences the maghemite within the impellers. This is realized by a setup designed for this purpose. Further, the Halbach array in this setup is motor-driven, which allows precise adjustment of the rotation speed both clockwise and counterclockwise. Figure 4b shows the time series of an in-chip clockwise rotation of the impeller-shaped microgels at a speed of 2 rpm (Video S4, Supporting Information) induced by the surrounding rotating Halbach array. The adapted fabrication procedure, the post-treatment, and the rotation conditions enable a homogeneous and even microgel rotation. In addition to observations of the rotation of the magnetic microgels, micro particle tracking velocimetry (µPTV) analysis were performed, investigating the fluid

movement induced by the rotating impellers. In Figure 4c, single fluorescent particles in the fluid and their velocities are shown. The microgel impellers and pillars are schematically illustrated. Near the microgel impellers, rotating movements of the measured particles are observed in circular flow patterns. Figures 4c and 4d show different analyses of the same rotation experiment, velocities of individual particles, and a velocity field, respectively. The rotation speed of the magnetic field ω_{MF} was set to 15 rpm and a pressure of about 1 bar was applied on both sides of the microfluidic channel. Figure 4d demonstrates that the magnetically induced microgel rotation impacts the surrounding fluid inside the microfluidic chip. A field with 12 rotating microgels is displayed, showing the same section as in Figure 4c. In the center of each microgel, at the position of the fixed PDMS pillars, no particle movement is detected. Particle velocities up to 20 μm s^{-1} around the pillars, however, indicate mixing of the fluid in the region of the microgel impellers and even slightly beyond. An average diameter of about 160 μm around the pillars is effected by the rotating impellers, which is 60% larger than the outer diameter of the single impeller. The highest velocities are detected at the impeller body in their arm regions. The tracer particle movement decreases with increasing distance from the microgel. Between the rotating impeller-shaped microgels, nearly no fluid movement is present, demonstrating the effect of the flow being induced by the magnetic actuated rotation.

In the future, the field of mixing can be further increased by adapting the pillar arrangement, varying their distance or the pattern. Therefore, the microfluidic master design can be easily changed. Like this, a locally distributed and potentially more extensive mixing can be achieved in future investigations. Moreover, the microgel shape can easily be varied by changing the transparency mask in the SFL setup. Hence, the fluid displacement can be increased by optimizing the impeller shape of the microgels. Exemplary improved shapes are shown in Figure S8(II–V), Supporting Information. Furthermore, the developed actuable microfluidic system might have potential for additional applications besides the presented mixing, such as microfluidic pumping. A proof of concept of particle pumping is performed including a novel microfluidic chip design and first rotation experiments, shown in Figure S9 and Video S5, Supporting Information.

In conclusion, a stable and reproducible actuable microfluidic system was developed for spatio-temporal flow control. Magnetic microgels were produced at precise positions in a microfluidic device by polymerization around fixed pillars. This novel system is generated in one single step by polymerizing the microgels directly at their final position without further steps. The rotation of these magnetic impeller-shaped microgels is induced by the rotation of an external magnetic field of a Halbach array, causing actuation of the surrounding fluid. While there are some limitations remaining in the system, it demonstrates the potential of precisely integrating magnetic actuators with a strong magnetic moment as actuable microfluidic elements.

3. Conclusion

This work presents a detailed study of magnetic anisometric microgels and introduces a novel platform where architectured complex-shaped microgels can be used to control and guide flow by changing their position through an external magnetic field. The magnetic response of the microgels was achieved by integrating maghemite nanospindles in the reaction solution during the fabrication process via stop-flow lithography. A contactless actuation of the microgels was enabled using an external magnetic field. The magnetic responsiveness of these microgels was investigated under a rotating magnetic field. Thereby, the influences of maghemite alignment, polymerization parameter, microgel shape, maghemite content, and magnetic field strength on the microgel actuation were studied. In addition to the analysis of freely rotating magnetic microgels, these were integrated into a microfluidic chip, creating an actuable microfluidic system. This system was developed in a one-step process where the microgels are directly fabricated in a microfluidic chip containing PDMS pillars serving as fixed rotation axes. In the case of an impeller shape without an inner diameter, the hydrophilic microgels are tightly located around hydrophobic PDMS pillars. The gap between the static pillars and the rotating microgels results from the oxygen inhibition layer surrounding the PDMS pillars, ensuring stable microgel rotations around the axes. These integrated magnetic impeller-shaped microgels actively mixed their surrounding fluid inside a microfluidic channel, thus enabling spatio-temporal flow control remotely actuated by a rotating magnetic field.

The SFL-fabricated magnetic microgels together with the concept of fixing them in space while keeping them rotational free represent a novel versatile platform. One could envision the use of the microgels for tissue engineering due to their magnetic responsiveness, biocompatibility, and custom design in any elongated 2D shape. Future studies need to be dedicated to their assembly into scaffolds to test the influence of the in-built macroporosity and directionality on cell growth and the actuation patterns on cell proliferation. The magnetic microgels also may be utilized for future biomechanical analysis of proliferating tissue and other mechanobiological applications. Furthermore, magnetic actuation in a rotating field at the single microgel level may allow mixing at the micro-scale and the use of the magnetic microgels for micro-rheometry to study complex fluids. Finally, the strategy to precisely position the axis of rotation of microgels in a microfluidic chip offers the possibility to create more advanced microfluidic designs with movable and actuable elements that could be adapted for various applications, from microfluidic valves and pumps to particle sorting.

4. Experimental Section

Synthesis and Characterization of Maghemite Nanospindles: The synthesis of the maghemite nanospindles is a multi-step process of preparing hematite nanospindles of a specific size and aspect ratio following a procedure previously described by Ocaña et al.[38] and converting them to maghemite by reduction to magnetite and reoxidation at high temperatures. The preparation is explained in more detail in a previous work.[23] The initial characterization of the maghemite nanospindles was carried out by various microscopy and scattering methods. The size of the nanoparticles investigated by transmission electron microscopy (Tecnai F20, FEI) reveals a length of 260 ± 29.1 nm and a diameter of 51.2 ± 6.0 nm. Previous works show that these nanoparticles exhibit a magnetic moment along their long axis and a saturation magnetization M_S of around 60 A m^2 kg^{-1}.[34] These properties result in a strong magnetic response and the formation of dipolar chains within a magnetic field. Further details on the nanoparticles and their response to magnetic fields

are discussed in Section S1, Supporting Information, and in a previous publication.[23]

Fabrication of Microfluidic Chips: The masters for microfluidic chips were produced using dip-in laser lithography with a two-photon lithography printer (Photonic Professional (GT) Printer, Nanoscribe GmbH, Eggenstein-Leopoldshafen, Germany).[39] By soft lithography,[40,41] microfluidic chips were casted from the masters. PDMS (Dow Corning, Sylgard 184 plus curing agent, 10:1 w/w) was used as chip material, being poured onto the master and cured at 60 °C overnight. After detaching, the cured PDMS form was perforated to achieve tubing holes, washed by sonication in isopropanol, and dried at atmospheric conditions overnight. Afterward, the PDMS form was bonded on a glass slide (VWR, 52 x 76 x 1 mm, cut to 25 x 25 x 1 mm) coated with PDMS (approx. 1 mm thick PDMS layer) by oxygen plasma activation of PDMS and glass slide (TePla 100 Plasma System, PVA).[39] Both microfluidic channels, for fabrication and for in-chip rotation, were 15 mm long (*x*-direction) and 900 µm wide (*y*-direction). Figure 4a shows a SEM (TM 3030 Plus, Hitachi) image of the channel for in-chip rotation which has a height of 20 µm (*z*-direction) in contrast to the 80 µm high fabrication channel. The pillars (diameters of 15 µm) were spaced in regular distances to each other of 209 µm in *x* and 241 µm in *y*-direction.

Preparation of Reaction Solution for SFL: The reaction solutions contained the pre-polymer PEGDA (average molecular weight of $M_n = 575$ Da, with 400–600 ppm MEHQ as inhibitor, Sigma Aldrich), initiator LAP (⩾ 95%, Sigma-Aldrich), and a water(HiPerSolv CHROMANORM, VWR)–maghemite mixture as solvent. The radical scavenger 4-methoxyphenole (MEHQ) (purum, ⩾ 98%, Sigma-Aldrich) was added to the reaction solution for the in-chip polymerization of microgels around pillars. For the preparation of the reaction solution, the pre-polymer and the initiator were weight out into separate vials. The pre-polymer was than thoroughly mixed with the ingredients of the solvent. The solvent was presented by a mixture of water and the concentrated maghemite suspension (2 g L^{-1}). The maghemite suspension was mixed and placed in an ultra sound bath for 5 min before adding it to the reaction solution. Subsequently, the pre-polymer solvent mixture was added onto the initiator powder and mixed thoroughly. For in-chip polymerization, the radical scavenger was weighed out into a separate vial, and the pre-polymer solvent mixture was added onto the radical scavenger prior to admit the resulting mixture to the initiator powder.

Fabrication of Magnetic Microgels Using SFL: Microgels were fabricated from reaction solutions containing PEGDA (20 wt%), LAP (0.5 wt%), maghemite (≈0.08 wt%), and water. The maghemite content resulted from dissolving the concentrated maghemite solution in water (50:50 mixture). The stage setup shown in Figure 1a was used for the microgel fabrication using SFL.[17] The fabrications were carried out in three different forces of the magnetic field (2, 13, and 68 mT). Different mask shapes and pattern diameters were applied: circular rods (7 µm diameter), three-arm impellers (92 µm outer diameter), and snowflakes (100 µm outer diameter). The polymerizations were carried out with varying radiant power and exposure times depending on the mask patterns: rods (1280 mW, 50 ms), impellers (930 mW, 50 ms), and snowflakes (1280 mW, 60 ms). For the impeller mask, two sets of polymerization parameters were applied, one with a high radiant power and short exposure time (1270 mW, 120 ms), the other with a low radiant power and long exposure time (130 mW, 500 ms). Further, rod-shaped microgels were fabricated with and without applied magnetic field (13 mT) and impeller microgels were fabricated with varying maghemite contents (0.02 wt%, 0.04 wt%, and 0.06 wt% in addition to 0.08 wt%). After fabrication, the resulting microgel containing solution was diluted with water (1:1) to enhance further reaction and stored at 4 °C.

Analysis of Magnetic Response of Microgels: The prepared microgels were cleaned by repeated solvent exchange with water. Therefore, microgels were allowed to sediment for 30 min. The supernatant was removed and replaced with water. This procedure was repeated five times. To analyze the magnetic response of the microgels, experiments were conducted inside a rotating magnetic field. These were performed on a modified Axioscope (Carl Zeiss Microscopy Deutschland GmbH) with a rotational stage driven by a piezoelectric engine (PILine U651.03, Physik Instrumente [PI] GmbH & Co. KG). Custom-made circular Halbach arrays consisting of different numbers and sizes of neodymium magnets can be mounted on the rotating stage and were used to apply the magnetic field. With this setup, field strengths between 1–300 mT and rotations rates of 0.1–90 rpm are reached. Standard microscope glass slides (22 x 22 mm, VWR) used in the experiments were cleaned with isopropanol inside an ultrasonic bath for 15 min and treated in a ozone oven for additional 15 min. The microgel batch (9 µL) was sealed with two SecureSeal Spacers (Invitrogen), creating a well (0.24 mm height, 9 mm diameter). To analyze the magnetic response, cross-polarization microscopy was performed on microgels exposed to a rotating magnetic field. Therefore, videos (3600 frames, 100 fps) were recorded and analyzed regarding the intensity change caused by the maghemite chains inside the microgels. The image analysis was done with ImageJ[42] and a custom-written Matlab routine. For the mean values of ω_C around 20 microgels were investigated.

Fabrication of Magnetic Microgels Immobilized In-Chip: Microgels around pillars were polymerized in a reaction solution containing PEGDA (20 wt%), LAP (1 wt%), maghemite (≈0.08 wt%), MEHQ (0.5 wt%), and water. The three-arm impellers were fabricated using a magnetic field (13 mT), which was aligned to the microfluidic channel with the setup shown in Figure 1a. After fabrication, the reaction solution was exchanged against the flushing solution to avoid further polymerization inside the chip. The composition of the flushing solution was investigated to optimize the magnetic response capability of the microgels. The optimal flushing solution contains PEGDA (40 wt%), MEHQ (1 wt%), polyoxyethylene (20) sorbitan monolaurate (Tween-20) (0.05 v%, Merck), and water.

Analysis of Induced Flow by Immobilized Microgels: For the in-chip rotation analysis, a custom-made setup with a motor-driven Halbach array (68 mT) was used. The influence of the magnetically induced in-chip rotation of the microgels on the surrounding fluid was investigated by µPTV. This technique enables the quantification of fluid flows by tracking tracer particles. As tracers, fluorescent polystyrene microspheres (0.86 µm diameter, Rhodamine 6G dye, LaVision GmbH) were added to the flushing solution (0.07 v%). This seeded flushing solution was flushed into the microfluidic chip until it filled the whole channel. Afterward, the inlet pressure was increased to 1000 mbar and the outlet pressure was raised until the fluid flow stopped. This procedure was visually observed through the stereomicroscope (SteREO Discovery.V20, Carl Zeiss Microscopy Deutschland GmbH) of the µPTV setup. After preparation, the rotation of the Halbach array was induced and investigations started. During the measurement, a high-frequency Nd:YAG laser (532 nm, DM150, Photonics Industries International Inc.) induced the fluorescent response of the tracer particles, while two high-speed cameras (Phantom VEO 710L, Vision Research Inc.) recorded their movement. The setup was controlled by the software DaVis (version: 10.0.5.47779, LaVision GmbH), which was also used for the image processing. With this software, particle tracks were processed to velocity fields, enabling the visualization of the fluid flow. A detailed description of the setup and the image post-processing is given in Stockmeier et al.[43]

Supporting Information

Supporting Information is available from the Wiley Online Library or from the author.

Acknowledgements

This work was financed by the Deutsche Forschungsgemeinschaft (DFG) within the SFB 985 "Functional Microgels and Microgel Systems" project B5 and financially supported by the Werner Siemens Foundation (Project TriggerINK). The µPTV measurements were conducted with a high-speed stereomicroscope PIV funded by the Major Research Instrumentation Program according to Art. 91b GG in the Research Building NW1481006 "NGP2—Center for Next Generation Processes and Products." M.W. acknowledges DFG funding through the Gottfried Wilhelm Leibniz Award 2019 (WE 4678/12-1) and the Alexander-von-Humboldt foundation. J.J.C. acknowledges financial support from the Exploratory Research Space of RWTH Aachen University (project StUpJP-049-18 and BioTrans012). The

authors thank Felix Stockmeier for conducting the μPTV measurements and post-processing, Julian Eigen for the SEM images, Andreas Falkenstein for the nanospindle conversion into maghemite, Meriem Saadli for the particle tracking performed on free rotating microgels, and Johann Savinsky for sample preparations.

Open access funding enabled and organized by Projekt DEAL.

Conflict of Interest

The authors declare no conflict of interest.

Author Contributions

L.S., H.J.M.W., and D.L.B. contributed equally to this work. L.S., H.J.M.W., and D.L.B.: conceptualization; formal analysis; investigation; methodology; project administration; supervision; validation; visualization; writing—original draft; writing—review and editing. V.H. and J.W.: investigation; methodology. J.J.C., M.W., and J.L.: conceptualization; funding acquisition; project administration; resources; supervision; writing—review and editing.

Data Availability Statement

The data that support the findings of this study are available from the corresponding author upon reasonable request.

Keywords

flow control, maghemite spindles, magnetic actuation, microgels, stop-flow lithography

Received: February 9, 2023
Published online:

[1] X. Xia, C. M. Spadaccini, J. R. Greer, *Nat. Rev. Mater.* **2022**, *7*, 683.
[2] J. A. Jackson, M. C. Messner, N. A. Dudukovic, W. L. Smith, L. Bekker, B. Moran, A. M. Golobic, A. J. Pascall, E. B. Duoss, K. J. Loh, et al., *Sci. Adv.* **2018**, *4*, eaau6419.
[3] A. Aubret, Q. Martinet, J. Palacci, *Nat. Commun.* **2021**, *12*, 1.
[4] D. Han, C. Farino, C. Yang, T. Scott, D. Browe, W. Choi, J. W. Freeman, H. Lee, *ACS Appl. Mater. Interfaces* **2018**, *10*, 17512.
[5] J. Cui, T.-Y. Huang, Z. Luo, P. Testa, H. Gu, X.-Z. Chen, B. J. Nelson, L. J. Heyderman, *Nature* **2019**, *575*, 164.
[6] A. M. Schmidt, *Macromol Rapid Commun* **2006**, *27*, 1168.
[7] Q. Ze, X. Kuang, S. Wu, J. Wong, S. M. Montgomery, R. Zhang, J. M. Kovitz, F. Yang, H. J. Qi, R. Zhao, *Adv. Mater.* **2020**, *32*, 1906657.
[8] T. Xu, J. Zhang, M. Salehizadeh, O. Onaizah, E. Diller, *Sci. Robot.* **2019**, *4*, eaav4494.
[9] D. J. Beebe, J. S. Moore, J. M. Bauer, Q. Yu, R. H. Liu, C. Devadoss, B. H. Jo, *Nature* **2000**, *404*, 588.
[10] D. T. Eddington, D. J. Beebe, *Adv. Drug Deliv. Rev.* **2004**, *56*, 199.
[11] A. Terray, J. Oakey, D. W. Marr, *Science* **2002**, *296*, 1841.
[12] K. Han, C. W. Shields IV, N. M. Diwakar, B. Bharti, G. P. López, O. D. Velev, *Sci. Adv.* **2017**, *3*, e1701108.
[13] S. Maruo, H. Inoue, *Appl. Phys. Lett.* **2006**, *89*, 144101.
[14] M. Matteucci, F. Perennes, B. Marmiroli, P. Miotti, L. Vaccari, A. Gosparini, A. Turchet, E. Di Fabrizio, *Microelectronic Eng* **2006**, *83*, 1288.
[15] K. F. Lei, W. C. Law, Y.-K. Suen, W. J. Li, Y. Yam, H. P. Ho, S.-K. Kong, *Proc Inst Mech Eng H* **2007**, *221*, 129.
[16] F. A. Plamper, W. Richtering, *Acc. Chem. Res.* **2017**, *50*, 131.
[17] H. J. Wolff, J. Linkhorst, T. Göttlich, J. Savinsky, A. J. Krüger, L. de Laporte, M. Wessling, *Lab Chip* **2020**, *20*, 285.
[18] M. Karg, A. Pich, T. Hellweg, T. Hoare, L. A. Lyon, J. J. Crassous, D. Suzuki, R. A. Gumerov, S. Schneider, I. I. Potemkin, W. Richtering, *Langmuir* **2019**, *35*, 6231.
[19] N. Weigel, Y. Li, A. Fery, J. Thiele, *COCIS* **2022**, *64*, 101673.
[20] S. Babu, I. Chen, S. Vedaraman, J. Gerardo-Nava, C. Licht, Y. Kittel, T. Haraszti, J. Di Russo, L. De Laporte, *Adv. Funct. Mater.* **2022**, 2202468.
[21] J. C. Rose, M. Cámara-Torres, K. Rahimi, J. Köhler, M. Möller, L. De Laporte, *Nano Lett.* **2017**, *17*, 3782.
[22] J. C. Rose, M. Fölster, L. Kivilip, J. L. Gerardo-Nava, E. E. Jaekel, D. B. Gehlen, W. Rohlfs, L. De Laporte, *Polym. Chem.* **2020**, *11*, 496.
[23] D. L. Braunmiller, S. Babu, D. B. Gehlen, M. Seuß, T. Haraszti, A. Falkenstein, J. Eigen, L. De Laporte, J. J. Crassous, *Adv. Funct. Mater.* **2022**, *32*, 2202430.
[24] Y. Chandorkar, A. Castro Nava, S. Schweizerhof, M. Van Dongen, T. Haraszti, J. Köhler, H. Zhang, R. Windoffer, A. Mourran, M. Möller, L. De Laporte, *Nat. Commun.* **2019**, *10*, 1.
[25] S. D. Oberdick, G. Zabow, *ACS Appl. Polym. Mater.* **2020**, *2*, 846.
[26] J. Nunes, K. P. Herlihy, L. Mair, R. Superfine, J. M. DeSimone, *Nano Lett.* **2010**, *10*, 1113.
[27] H. Lee, J. Kim, H. Kim, J. Kim, S. Kwon, *Nat. Mater.* **2010**, *9*, 745.
[28] S. K. Suh, S. C. Chapin, T. A. Hatton, P. S. Doyle, *Microfluid. Nanofluidics* **2012**, *13*, 665.
[29] N. Hakimi, S. S. Tsai, C.-H. Cheng, D. K. Hwang, *Adv. Mater.* **2014**, *26*, 1393.
[30] S. K. Suh, K. Yuet, D. K. Hwang, K. W. Bong, P. S. Doyle, T. A. Hatton, *J. Am. Chem. Soc.* **2012**, *134*, 7337.
[31] L. M. Sanchez, D. G. Actis, J. S. Gonzalez, P. M. Zélis, V. A. Alvarez, *J. Nanoparticle Res.* **2019**, *21*, 64.
[32] M. Deuflhard, D. Eberbeck, P. Hietschold, N. Wilharm, M. Mühlberger, R. P. Friedrich, C. Alexiou, S. G. Mayr, *Phys. Chem. Chem. Phys.* **2019**, *21*, 14654.
[33] M. Saadli, D. L. Braunmiller, A. Mourran, J. J. Crassous, *Small* **2023**, *n/a*, 2207035.
[34] V. Malik, A. Pal, O. Pravaz, J. J. Crassous, S. Granville, B. Grobety, A. M. Hirt, H. Dietsch, P. Schurtenberger, *Nanoscale* **2017**, *9*, 14405.
[35] I. Bouhid de Aguiar, K. Schroën, M. Meireles, A. Bouchoux, *Colloids Surf. A Physicochem. Eng. Asp.* **2018**, *553*, 406.
[36] A. Cavallo, M. Madaghiele, U. Masullo, M. G. Lionetto, A. Sannino, *J. Appl. Polym. Sci.* **2017**, *134*, 2.
[37] R. Sadeghi, F. Jahani, *J. Phys. Chem. B* **2012**, *116*, 5234.
[38] M. Ocaña, M. P. Morales, C. J. Serna, *J. Colloid Interface Sci.* **1999**, *212*, 317.
[39] J. Lölsberg, J. Linkhorst, A. Cinar, A. Jans, A. J. Kuehne, M. Wessling, *Lab Chip* **2018**, *18*, 1341.
[40] P. Kim, K. W. Kwon, M. C. Park, S. H. Lee, S. M. Kim, K. Y. Suh, *BioChip J.* **2008**, *2*, 1.
[41] Y. Xia, G. M. Whitesides, *Angew. Chem., Int. Ed.* **1998**, *37*, 550.
[42] M. Abramoff, P. Magalhães, S. J. Ram, *Biophotonics Int.* **2003**, *11*, 36.
[43] F. Stockmeier, M. Schatz, M. Habermann, J. Linkhorst, A. Mani, M. Wessling, *MethodsX* **2022**, *9*, 101814.